UC Davis

UC Davis Previously Published Works

Title

Stabilization of a Metastable Fibrous Bi21.2(1)(Mn1–x Co x)20 Phase with Pseudo-Pentagonal Symmetry Prepared Using a Bi Self-Flux

Permalink

https://escholarship.org/uc/item/1qj5n6vn

Journal

Chemistry of Materials, 28(23)

ISSN

0897-4756

Authors

Thimmaiah, Srinivasa
Taufour, Valentin
Saunders, Scott
et al.

Publication Date

2016-12-13

DOI

10.1021/acs.chemmater.6b04505

Peer reviewed

eScholarship.org Powered by the California Digital Library
University of California

CHEMISTRY OF MATERIALS

Communication

pubs.acs.org/cm

Stabilization of a Metastable Fibrous $Bi_{21.2(1)}(Mn_{1-x}Co_x)_{20}$ Phase with Pseudo-Pentagonal Symmetry Prepared Using a Bi Self-Flux

Srinivasa Thimmaiah,*[,†] Valentin Taufour,[†,§] Scott Saunders,[§] Stephen March,[§] Yuemei Zhang,[‡] Matthew J. Kramer,[†,∥] Paul C. Canfield,[†,§] and Gordon J. Miller[†,‡]

[†]The Ames Laboratory, U.S. Department of Energy, Iowa State University, Ames, Iowa 50011, United States

[‡]Department of Chemistry, Iowa State University, Ames, Iowa 50011, United States

[§]Department of Physics and Astronomy, Iowa State University, Ames, Iowa 50011, United States

[∥]Department of Materials Science and Engineering, Iowa State University, Ames, Iowa 50011, United States

Supporting Information

Permanent magnets are exceptionally critical for many environmentally friendly, energy harvesting technologies in our energy demanding modern world.[1,2] In particular, rare earth (RE) based permanent magnets such as $Nd_2Fe_{14}B_2$[3−5] and $SmCo_5$[6,7] are extensively used for energy conversion purposes, mainly in high-power generators and motors found in wind turbines and electric vehicles, due to their very high energy product (BH_{max}) and lightweight. In particular, demand for RE-based permanent magnets has been growing exponentially in recent years. Therefore, to ease reliance on RE-based permanent magnets, development of low cost alternative materials that have high energy products and high Curie temperatures are critical for future sustainability. Mn-based[8] intermetallic compounds are examples gaining ground as an effective alternative, especially the ferromagnetic, low temperature (LT) BiMn phase adopting the NiAs-type structure and exhibiting a large uniaxial magnetic anisotropy ($K = 2.2 \times 10^7$ erg cm^{-3} at 500 K). At temperatures exceeding 300 K, LT-BiMn shows remarkably high coercivity, which is even larger than that for $Nd_2Fe_{14}B_2$ magnets, making LT-BiMn suitable for high temperature applications.[9−12] However, at 633 K ferromagnetic LT-BiMn transforms to a paramagnetic, high-temperature phase (HTP),[13,14] which, upon rapid quenching, results in a ferromagnetic phase that shows an interesting magneto-optical property[15−18] applicable for magneto-optical memory devices. There are two structural transitions reported for LT-BiMn: one at ca. 100 K where spin reorientation occurs;[19] and another above its Curie or decomposition temperature (633 K). Theoretical calculations suggested that partial replacement of Mn by other transition metals could stabilize its structure in the hexagonal NiAs-type, which is essential for retaining the magnetic properties as well as increasing the magnetic anisotropy,[20,21] but experimental results reveal a change in crystal structure upon doping.[22] Herein, we report a new phase $Bi_{21.2(1)}(Mn_{1-x}Co_x)_{20}$ ($x \sim 0.15$) that was discovered during systematic substitution of 3*d* and 4*d*[22] transition metals for Mn in LT-BiMn (NiAs-type) as a theoretically predicted strategy to increase magnetic anisotropy and stabilization of NiAs-type structure at elevated temperature.

Crystals of a new metastable Co-doped BiMn phase were grown using Bi as a self-flux at 280 °C.[23] Figure 1 shows the soft and highly fibrous nature of these crystals, which split into submicron-size strands upon applied pressure. According to

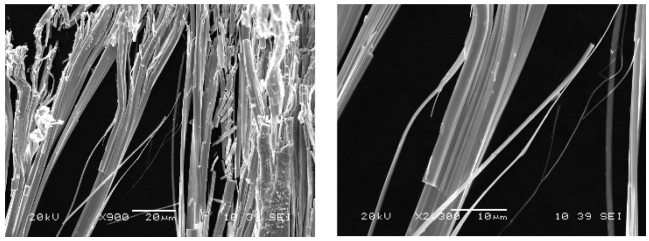

Figure 1. SEM micrographs of $Bi_{21.2(1)}(Mn_{1-x}Co_x)_{20}$ crystals showing fibrous morphology.

DSC, the Co-doped BiMn phase decomposes endothermically on heating around 168 °C, with no evidence of formation of a new phase during cooling (see Supporting Information, Figure S2). This clearly indicates the metastable nature of the new phase. On the contrary, typical high-temperature reaction conditions of a sample with nominal composition of $Mn_{43}Co_7Bi_{50}$ resulted in the hexagonal NiAs-type structure (a = 4.2907(1) Å, c = 6.1199(3) Å),[24] which decomposes around 355 °C (see Supporting Information, Figure S4) upon heating.

Single crystal X-ray diffraction revealed that the new phase crystallizes in orthorhombic symmetry, space group *Imma*, and the refined composition is $Bi_{21.2(1)}(Mn_{1-x}Co_x)_{20}$ ($x \sim 0.15$). However, the positions of Co atoms in the crystal structure could not be established precisely due to the similar X-ray scattering contrasts of Mn and Co. Thus, wavelength-dispersive X-ray spectroscopy was employed to estimate the amount of Co to be 7(1) at.% in the structure. To evaluate any possible chemical ordering of Co in the structure, we have calculated total energies for two different compositions, each with three different coloring schemes, using VASP. The calculated energy differences among these various coloring models were found to be negligible (11−64 meV/cell or 0.26−1.52 meV/atom) (see Supporting Information, Figure S9), indicating low probability for chemical ordering of Co atoms in the structure under these synthetic conditions. Therefore, we can conclude that Co atoms are essentially randomly mixed with Mn atoms at the 3*d* metal positions.

Received: October 21, 2016
Revised: November 15, 2016
Published: November 15, 2016

ACS Publications © 2016 American Chemical Society

DOI: 10.1021/acs.chemmater.6b04505
Chem. Mater. 2016, 28, 8484−8488

As illustrated in Figure 2, the orthorhombic crystal structure of $Bi_{21.2(1)}(Mn_{1-x}Co_x)_{20}$ exhibits 1D $_\infty^1[Bi_{0.32}@T_5@Bi_5]$ (T =

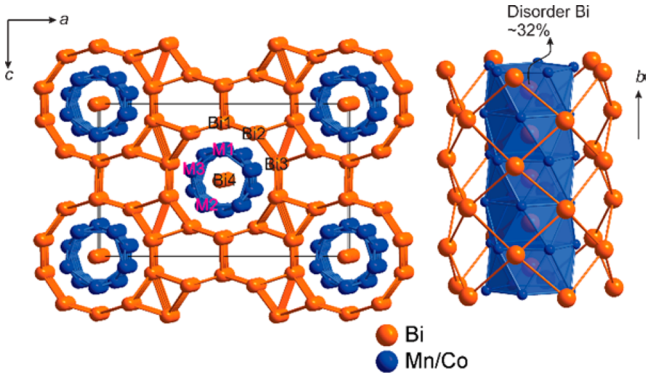

Figure 2. Crystal structure of $Bi_{21.2(1)}(Mn_{1-x}Co_x)_{20}$, showing doubled walled stuctural arrangement of Bi and Mn/Co atoms along [0 1 0] direction.

Mn/Co) columns along the [010] direction arranged in a hexagonal rod packing manner with respect to the *ac*-plane. The center of each column is occupied by a Bi atom whose site occupancy was freely refined to 32(1)%. The arrangement of the atoms in each column mimics local pentagonal symmetry, although long-range ordering of pentagonal symmetry is disrupted by the hexagonal rod-packing of the columns, as observed from reflections in reciprocal space (see Supporting Information, Figure S5). Although the refined electron density inside these columns can also be interpreted as a fully occupied Mn/Co (T) position, T−T distances between this site are too short (2.3035(5) Å) to be considered as fully occupied by a Mn/Co mixture. Therefore, atoms in the center have been treated as partially occupied by Bi atoms, an assumption that corroborates well with similar features observed for $Bi_{28}Ni_{25}$[25] and Bi_8Ni_8S.[26] The shell of T atoms around the disordered central Bi atoms forms a pentagonal antiprismatic column along the [010] direction. T−T distances range from 2.690(3) to 2.777(5) Å, which are rather short compared to Mn−Mn distances in ferromagnetic LT-BiMn (3.0456 Å). The Mn−Mn distances play a critical role for the onset of ferromagnetism in NiAs-type structures as well as other rare-earth based intermetallic compounds due to direct-exchange interactions.[22,27−32] Furthermore, each plane of pentagons of T5 atoms is surrounded by Bi atoms in the staggered manner creating a local pentagonal symmetry. The Bi−Bi distances in the structure range between 3.5056(10) and 3.6632(12) Å, which are well within the range observed for BiMn[13,14] and BiNi.[25,33]

Analysis of the X-ray powder diffraction pattern indicates that a noticeable amount of unreacted Bi flux occurs as a minority product, along with $Bi_{21.2(1)}(Mn_{1-x}Co_x)_{20}$ (see Supporting Information, Figure S1), but there is no evidence for the presence of LT-BiMn or the formation of any superstructure due to partially ordered Bi atoms inside the columns. LT-BiMn is a very stable phase that forms rapidly in the absence any additional transition metals or metalloids (<10 at. %). These added transition metals or metalloids frequently trigger the formation of a superstructure by incorporating into empty trigonal bipyramidal sites of the NiAs-type structure, thereby triggering complex superstructures that can be commensurate or incommensurately modulated.[34−38]

The structural motif of $Bi_{21.2(1)}(Mn_{1-x}Co_x)_{20}$ is very similar to other metastable phases $Bi_{28}Ni_{25}$[25] and Bi_8Ni_8S.[26] Both of these are obtained via pseudomorphic transformation by reduction of the corresponding subiodide, although they decompose irreversibly upon heating to NiAs-type BiNi at 145 and 180 °C, respectively. In our case, crystals of $Bi_{21.2(1)}(Mn_{1-x}Co_x)_{20}$ can be obtained directly at 280 °C using the Bi self-flux, which is a useful technique to arrest many metastable phases.[39−41] These structural features are also closely related to those in $Na_{2.8}Cu_5Sn_{5.6}$,[42] in which the inner shell is composed of Cu atoms, the outer shell by Sn atoms, and a disordered arrangement of Sn atoms occupies the center of the columns.

Electronic structure calculations were performed on an ordered structure model "$Bi_{22}Mn_{20}$" using TB-LMTO-ASA. Figure 3a,c shows, respectively, the electronic density of states

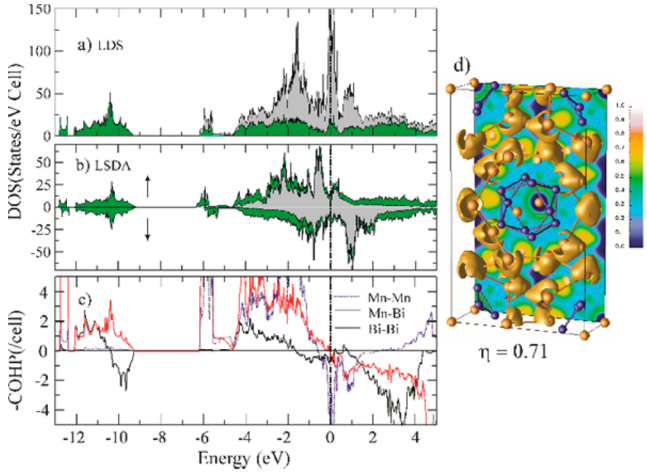

Figure 3. DOS and COHP curves for "$Bi_{22}Mn_{20}$" in LDA and LSDA using LMTO-ASA. The Fermi level (0 eV) for the calculated composition is marked by the dashed line. Positive −COHP values are bonding states; negative −COHP values are antibonding states. (a and b) DOS (LDA and LSDA) curve with contributions from Mn (gray) and Bi (green) is highlighted. Mn 3*d* and 4*s* and Bi 6*s* and 6*p* orbitals make the principal contributions to all occupied states. (c) Calculated COHP curves for different interactions from LDA. (d) ELF isosurface at value of ELF = 0.71 suggesting the highly localized, lone-pair like basins around Bi atoms.

(DOS) various metal−metal crystal orbital Hamilton populations (COHP) curves using LDA. The region near the Fermi level is mainly dominated by Mn 3*d* with some contributions from Bi 6*p* orbitals. The Bi 6*s* states, centered at −11 eV, broaden slightly by ca. 3.5 eV due to weak interactions with Mn 4*s* orbitals. Evaluation of the electron localization function (ELF) also reveals the existence of a nearly spherical, localized electronic basin around Bi atoms, indicative of a lone pair on the Bi atoms as shown in Figure 3d (ELF isovalue = 0.71). A small extent of valence *s*−*p* mixing at Bi can be seen in the Bi PDOS, an outcome that is typical for group 15 elements.[43,44] The Fermi level falls within a narrow peak of the DOS, which suggests a potential electronic instability that can be relieved through spin-polarization leading to ferromagnetic or antiferromagnetic ordering in the material.[45] In the corresponding COHP curves, this peak originates from Mn−Mn antibonding interactions, whereas the Mn−Bi interactions are optimized and Bi−Bi interactions are essentially nonbonding. Furthermore, analysis of the integrated COHP (ICOHP) values over all

DOI: 10.1021/acs.chemmater.6b04505
Chem. Mater. 2016, 28, 8484−8488

occupied states revealed that Mn−Mn and Mn−Bi interactions constitute 40.9% and 54.1%, respectively for bonding, whereas Bi−Bi contacts contribute only 5%.

Upon spin polarization, the DOS curves, shown in Figure 3b, split into majority- and minority-spin states and the Fermi level no longer resides within a sharp peak, but instead falls in a pseudogap. Moreover, the spin-polarized (LSDA) calculation lowers the total energy of the system by 5.3 eV per unit cell compared to nonspin polarized (LDA) calculation. The DOS projections reveal that the Mn 3*d* states show significant exchange splitting, whereas the Bi 6*p* states show small exchange splitting. Several different magnetic models were examined, but they converged to one of two different ferrimagnetic arrangements with the majority of magnetic moments on the Mn sites and small moments on the Bi sites. In the corresponding spin-polarized COHP curves, Mn−Mn and Mn−Bi interactions are no longer antibonding at the Fermi level (see Supporting Information, Figure S7). On the basis of these computational results, we anticipate some magnetic ordering in $Bi_{21.2(1)}(Mn_{1-x}Co_x)_{20}$ at low temperature. However, we have been unable to confirm these properties due to the highly fibrous nature of the crystals and the presence of a small amount of unreacted Bi flux in the final product.

In summary, the new metastable phase $Bi_{21.2(1)}(Mn_{1-x}Co_x)_{20}$ ($x \sim 0.15$) can be synthesized using a flux method in the presence of a small amount of cobalt. The arrangement of the atoms in the structure mimics pentagonal symmetry. Total energy calculations using VASP revealed that no chemical ordering of cobalt occurs in that structure, i.e., Co is randomly distributed on the Mn sites, and that low-temperature magnetic ordering is possible.

Single crystals of Co-doped BiMn were grown using an approximately 5 g mixture of Co (99.9%), Mn (99.995% ROC/RIC), and Bi (99.99% Alfa Aesar) placed into a 2 mL alumina crucible with a molar ratio of Mn:Co:Bi = $(10 - x):x:90$ (x = 0.0, 0.5, 1.0, 2.0). The crucible with the elements was sealed in a fused silica ampule under an argon atmosphere, which was then heated to 1150 °C, held at 1150 °C for 5 h, and then cooled to 390 °C over 5 h. Samples were kept at 390 °C for 2 h, and then cooled at a rate of approximately 1 °C per hour to 280 °C. Once the temperature was stabilized at 280 °C, the excess Bi was removed by centrifugation.

X-ray powder diffraction data were collected on a Rigaku Miniflex diffractrometer operating in a Bragg−Brentano geometry using Cu Kα radiation at room temperature. Because of the soft nature of product, the crystals were immersed in liquid nitrogen for a few minutes before grinding into powder. The powder was evenly spread over the zero background single crystal silicon wafer sample holder with the aid of a thin film of Dow Corning high vacuum grease.

Elemental analysis of the samples was performed using wavelength-dispersive X-ray spectroscopy (WDS) in a JEOL JXA-8200 electron probe microanalyzer. WDS data were collected and averaged from multiple points on a clear and shiny as-grown surface for determination of the sample composition, i.e., regions with residual Bi flux were avoided. Scanning electron micrographs were recorded using a JEOL 5910LV scanning electron microscope.

Single crystal diffraction data were collected on a Bruker APEX II CCD diffractometer equipped with graphite monochromator using Mo Kα radiation at room temperature (60 s/frame and 50 mm detector distance). An empirical absorption correction was applied using the program SADABS. The crystal structure was solved using SHELXT and refined on F^2 by means of full-matrix least-squares methods using SHEXL2014,[46−48] with anisotropic displacement parameters for all atoms. During structure refinement all the mixed Mn/Co positions were refined as Mn. Crystal data: orthorhombic *Imma*; a = 19.067(4) Å, b = 4.6071(10) Å, c = 11.583(4) Å, V = 1017.4(4) Å^3, R1/wR2 = 0.0526/0.0938 for the observed data and R1/wR2 = 0.1087/0.1099 for all data.

Total energy calculations were performed using the projector augmented wave (PAW) method of Blöchl[49,50] coded in the Vienna *ab initio* simulation package (VASP).[51] All VASP calculations employed the generalized gradient approximation (GGA) with exchange and correlation treated by the Perdew−Burke−Enzerhoff (PBE) functional.[52] The cutoff energy for the plane wave calculations was set to 500 eV and the Brillouin zone integration was carried out using a 13 × 3 × 5 k-point mesh. The density of states (DOS), crystal overlap Hamilton populations (COHP),[53] band structures and the electron localization function (ELF)[54] were calculated using the Stuttgart LMTO-ASA program.[55] The calculations were performed on "$Bi_{22}Mn_{20}$" in space group *Pmna* with Bi vacancies on either the 2*a* or 2*d* sites, and "$Bi_{24}Mn_{20}$" in space group *Imma* with no vacancies.

■ ASSOCIATED CONTENT

Supporting Information

The Supporting Information is available free of charge on the ACS Publications website at DOI: 10.1021/acs.chemmater.6b04505.

Additional experimental details; crystallographic data; atomic coordinates; powder XRD data; DSC thermogram; DOS, and band structure (PDF)

Data for $Bi_{21.2}Mn_{20}$ (CIF)

■ AUTHOR INFORMATION

Corresponding Author

*S. Thimmaiah. E-mail: srini@iastate.edu.

ORCID

Srinivasa Thimmaiah: 0000-0001-8875-4883

Notes

The authors declare no competing financial interest.

■ ACKNOWLEDGMENTS

We thank Dr. Warren Straszheim for doing WDS on various samples. S.T., and G.J.M., were supported by the U.S. Department of Energy, Office of Basic Energy Sciences, Division of Materials Sciences and Engineering. V.T., S.S., S.M., M.J.K., and P.C.C. were supported by the Critical Materials Institute, an Energy Innovation Hub funded by the U.S. Department of Energy, Office of Energy Efficiency and Renewable Energy, Advanced Manufacturing Office. This work was carried out at the Ames Laboratory, which is operated for the U.S. Department of Energy by Iowa State University under Contract No. DE-AC02-07CH11358.

■ REFERENCES

(1) Gutfleisch, O.; Willard, M. A.; Brück, E.; Chen, C. H.; Sankar, S. G.; Liu, J. P. Magnetic Materials and Devices for the 21st Century: Stronger, Lighter, and More Energy Efficient. *Adv. Mater.* **2011**, *23*, 821−842.

DOI: 10.1021/acs.chemmater.6b04505
Chem. Mater. 2016, 28, 8484−8488

(2) Gschneidner, K. A., Jr.; Pecharsky, V. K.; Tsokol, A. O. Recent developments in magnetocaloric materials. *Rep. Prog. Phys.* **2005**, *68*, 1479−1539.
(3) Croat, J. J.; Herbst, J. F.; Lee, R. W.; Pinkerton, F. E. Pr-Fe and Nd-Fe-based materials: A new class of high-performance permanent magnets (invited). *J. Appl. Phys.* **1984**, *55*, 2078−2082.
(4) Sagawa, M.; Fujimura, S.; Togawa, N.; Yamamoto, H.; Matsuura, Y. New material for permanent magnets on a base of Nd and Fe (invited). *J. Appl. Phys.* **1984**, *55*, 2083−2087.
(5) Kirchmayr, H. R. Permanent magnets and hard magnetic materials. *J. Phys. D: Appl. Phys.* **1996**, *29*, 2763−2778.
(6) Strnat, K.; Hoffer, G.; Olson, J.; Ostertag, W.; Becker, J. J. A family of new cobalt-base permanent magnet materials. *J. Appl. Phys.* **1967**, *38*, 1001−1002.
(7) Buschow, K. H. J.; Van Der Goot, A. S. Intermetallic compounds in the system samarium-cobalt. *J. Less-Common Met.* **1968**, *14*, 323−328.
(8) Coey, J. M. D. New permanent magnets; manganese compounds. *J. Phys.: Condens. Matter* **2014**, *26*, 064211.
(9) Ly, V.; Wu, X.; Smillie, L.; Shoji, T.; Kato, A.; Manabe, A.; Suzuki, K. Low-temperature phase MnBi compound: A potential candidate for rare-earth free permanent magnets. *J. Alloys Compd.* **2014**, *615*, S285−S290.
(10) Kirkeminde, A.; Shen, J.; Gong, M.; Cui, J.; Ren, S. Metal-Redox Synthesis of MnBi Hard Magnetic Nanoparticles. *Chem. Mater.* **2015**, *27*, 4677−4681.
(11) Kharel, P.; Skomski, R.; Lukashev, P.; Sabirianov, R.; Sellmyer, D. J. Spin correlations and Kondo effect in a strong ferromagnet. *Phys. Rev. B: Condens. Matter Mater. Phys.* **2011**, *84*, 014431.
(12) Rao, N. V. R.; Gabay, A. M.; Hadjipanayis, G. C. Anisotropic fully dense MnBi permanent magnet with high energy product and high coercivity at elevated temperatures. *J. Phys. D: Appl. Phys.* **2013**, *46*, 062001.
(13) Andresen, A.; Hälg, W.; Fischer, P.; Stoll, E. The Magnetic and Crystallographic Properties of MnBi Studied by Neutron Diffraction. *Acta Chem. Scand.* **1967**, *21*, 1543−1554.
(14) Andresen, A. F.; Engebretsen, J. E.; Refsnes, J. Neutron diffraction investigations on quenched MnBi and MnBi0.9Sb0.1. *Acta Chem. Scand.* **1972**, *26*, 175−190.
(15) Di, G. Q.; Uchiyama, S. Optical and magneto-optical properties of MnBi film. *Phys. Rev. B: Condens. Matter Mater. Phys.* **1996**, *53*, 3327−3335.
(16) Harder, K.-U.; Menzel, D.; Widmer, T.; Schoenes, J. Structure, magnetic, and magneto-optical properties of MnBi films grown on quartz and (001)GaAs substrates. *J. Appl. Phys.* **1998**, *84*, 3625−3629.
(17) Antropov, V. P.; Antonov, V. N.; Bekenov, L. V.; Kutepov, A.; Kotliar, G. Magnetic anisotropic effects and electronic correlations in MnBi ferromagnet. *Phys. Rev. B: Condens. Matter Mater. Phys.* **2014**, *90*, 054404.
(18) Esho, S.; Nagao, M. Optical and Magneto-Optical Properties of MnBi Films. *Jpn. J. Appl. Phys.* **1974**, *13*, 445−450.
(19) McGuire, M. A.; Cao, H.; Chakoumakos, B. C.; Sales, B. C. Symmetry-lowering lattice distortion at the spin reorientation in MnBi single crystals. *Phys. Rev. B: Condens. Matter Mater. Phys.* **2014**, *90*, 174425.
(20) Zarkevich, N. A.; Wang, L.-L.; Johnson, D. D. Anomalous magneto-structural behavior of MnBi explained: A path towards an improved permanent magnet. *APL Mater.* **2014**, *2*, 032103.
(21) Hong, Y.-K.; Park, J.; Mryasov, O. N.; Kim, S.-G.; Kim, S.; Lee, J.; Abo, G. S.; Choi, C.-J.; Lee, J. Magnetic properties of MnBi based alloys: First-principles calculations for MnBi-Co and MnBi-Co-Fe cases. *AIP Adv.* **2013**, *3*, 052137.
(22) Taufour, V.; Thimmaiah, S.; March, S.; Saunders, S.; Sun, K.; Lamichhane, T. N.; Kramer, M. J.; Bud'ko, S. L.; Canfield, P. C. Structural and Ferromagnetic Properties of an Orthorhombic Phase of MnBi Stabilized with Rh Additions. *Phys. Rev. Appl.* **2015**, *4*, 014021.
(23) Canfield, P. C.; Fisk, Z. Growth of single crystals from metallic fluxes. *Philos. Mag. B* **1992**, *65*, 1117−1123.
(24) Göbel, H.; Wolfgang, E.; Harms, H. Properties of MnBi compounds partially substituted with Cu, Zn, Ti, Sb, and Te. I. Formation of mixed phases and crystal structures. *Phys. Stat. Sol. (a)* **1976**, *34*, 553−564.
(25) Kaiser, M.; Isaeva, A.; Ruck, M. A metastable metal with decagonal local symmetry obtained by low-temperature pseudomorphosis. *Angew. Chem., Int. Ed.* **2011**, *50*, 6178−6180.
(26) Kaiser, M.; Isaeva, A.; Skrotzki, R.; Schwarz, U.; Ruck, M. Metastable Bi8Ni8S by Reductive Pseudomorphosis of Bi8Ni8SI2. *Z. Anorg. Allg. Chem.* **2011**, *637*, 2026−2032.
(27) Seshu Bai, V.; Rajasekharan, T. Evidence of a critical Mn-Mn distance for the onset of ferromagnetism in NiAs type compounds. *J. Magn. Magn. Mater.* **1984**, *42*, 198−200.
(28) Willis, B. T. M.; Rooksby, H. P. Magnetic Transitions and Structural Changes in Hexagonal Manganese Compounds. *Proc. Phys. Soc., London, Sect. B* **1954**, *67*, 290−296.
(29) Murthy, N. S. S.; Begum, R. J.; Somanathan, C. S.; Murthy, M. R. L. N. Magnetic Structure of MnAlGe. *J. Appl. Phys.* **1969**, *40*, 1870−1871.
(30) Md Din, M. F.; Wang, J. L.; Cheng, Z. X.; Dou, S. X.; Kennedy, S. J.; Avdeev, M.; Campbell, S. J. Tuneable Magnetic Phase Transitions in Layered CeMn2Ge2-xSix Compounds. *Sci. Rep.* **2015**, *5*, 11288.
(31) Welter, R.; Venturini, G.; Ressouche, E.; Malaman, B. Neutron diffraction study of CeMn2Ge2, PrMn2Ge2 and NdMn2Ge2: evidence of dominant antiferromagnetic components within the (001) Mn planes in ferromagnetic ThCr2Si2-type manganese ternary compounds. *J. Alloys Compd.* **1995**, *218*, 204−215.
(32) Williams, T. J.; Taylor, A. E.; Christianson, A. D.; Hahn, S. E.; Fishman, R. S.; Parker, D. S.; McGuire, M. A.; Sales, B. C.; Lumsden, M. D. Extended magnetic exchange interactions in the high-temperature ferromagnet MnBi. *Appl. Phys. Lett.* **2016**, *108*, 192403.
(33) Ruck, M. Die Kristallstruktur von BiNi: eine komplexe Ausdünnungsvariante des InNi2-Typs. *Z. Anorg. Allg. Chem.* **1999**, *625*, 2050−2054.
(34) Lidin, S.; Petricek, V.; Stenberg, L.; Furuseth, S.; Fjellvåg, H.; Larsson, A.-K. The incommensurately modulated structure of NiBi. *Solid State Sci.* **2000**, *2*, 353−363.
(35) Elding-Ponten, M.; Stenberg, L.; Larsson, A.-K.; Lidin, S.; Stahl, K. Three NiAs-Ni2In type structures in the Mn-Sn system. *J. Solid State Chem.* **1997**, *129*, 231−241.
(36) Lidin, S.; Larsson, A.-K. A Survey of Superstructures in Intermetallic NiAs-Ni2In-Type Phases. *J. Solid State Chem.* **1995**, *118*, 313−322.
(37) Lidin, S.; Stenberg, L.; Elding-Pontén, M. The B8 type structure of Cu7In3. *J. Alloys Compd.* **1997**, *255*, 221−226.
(38) Müller, C. J.; Lidin, S.; de Debiaggi, S. R.; Deluque Toro, C. E.; Guillermet, A. F. Synthesis, Structural Characterization, and Ab Initio Study of Cu5+δIn2+xSb2−x: A New B8-Related Structure Type. *Inorg. Chem.* **2012**, *51*, 10787−10792.
(39) Kanatzidis, M. G.; Pöttgen, R.; Jeitschko, W. The Metal Flux: A Preparative Tool for the Exploration of Intermetallic Compounds. *Angew. Chem., Int. Ed.* **2005**, *44*, 6996−7023.
(40) Fisher, I. R.; Shapiro, M. C.; Analytis, J. G. Principles of crystal growth of intermetallic and oxide compounds from molten solutions. *Philos. Mag.* **2012**, *92*, 2401−2435.
(41) Shoemaker, D. P.; Hu, Y.-J.; Chung, D. Y.; Halder, G. J.; Chupas, P. J.; Soderholm, L.; Mitchell, J. F.; Kanatzidis, M. G. In situ studies of a platform for metastable inorganic crystal growth and materials discovery. *Proc. Natl. Acad. Sci. U. S. A.* **2014**, *111*, 10922−10927.
(42) Stegmaier, S.; Fässler, T. F. Na2.8Cu5Sn5.6: A Crystalline Alloy Featuring Intermetalloid {Sn0.6@Cu5@Sn5} Double-Walled Nanorods with Pseudo-Five-Fold Symmetry. *Angew. Chem., Int. Ed.* **2012**, *51*, 2647−2650.
(43) Rytz, R.; Hoffmann, R. Chemical Bonding in the Ternary Transition Metal Bismuthides Ti4TBi2 with T = Cr, Mn, Fe, Co, and Ni. *Inorg. Chem.* **1999**, *38*, 1609−1617.
(44) Seo, D.-K.; Hoffmann, R. What Determines the Structures of the Group 15 Elements? *J. Solid State Chem.* **1999**, *147*, 26−37.

DOI: 10.1021/acs.chemmater.6b04505
Chem. Mater. 2016, 28, 8484−8488

(45) Landrum, G. A.; Dronskowski, R. Ferromagnetism in Transition Metals: A Chemical Bonding Approach. *Angew. Chem., Int. Ed.* **1999**, *38*, 1389−1393.
(46) *APEX3*; Bruker AXS Inc.: Madison, WI, 2016.
(47) *SHELXTL*, v2016; Bruker AXS Inc.: Madison, WI, 2016.
(48) Sheldrick, G. Crystal structure refinement with SHELXL. *Acta Crystallogr., Sect. C: Struct. Chem.* **2015**, *71*, 3−8.
(49) Blöchl, P. E. Projector augmented-wave method. *Phys. Rev. B: Condens. Matter Mater. Phys.* **1994**, *50*, 17953−17979.
(50) Kresse, G.; Joubert, D. From ultrasoft pseudopotentials to the projector augmented-wave method. *Phys. Rev. B: Condens. Matter Mater. Phys.* **1999**, *59*, 1758−1775.
(51) Kresse, G.; Furthmüller, J. Efficient iterative schemes for *ab initio* total-energy calculations using a plane-wave basis set. *Phys. Rev. B: Condens. Matter Mater. Phys.* **1996**, *54*, 11169−11186.
(52) Perdew, J. P.; Burke, K.; Ernzerhof, M. Generalized Gradient Approximation Made Simple. *Phys. Rev. Lett.* **1996**, *77*, 3865−3868.
(53) Dronskowski, R.; Bloechl, P. E. Crystal orbital Hamilton populations (COHP): energy-resolved visualization of chemical bonding in solids based on density-functional calculations. *J. Phys. Chem.* **1993**, *97*, 8617−8624.
(54) Becke, A. D.; Edgecombe, K. E. A simple measure of electron localization in atomic and molecular systems. *J. Chem. Phys.* **1990**, *92*, 5397−5403.
(55) Jepsen, O.; Andersen, O. K. Calculated electronic structure of the sandwichd1 metals LaI2 and CeI2: Application of new LMTO techniques. *Z. Phys. B: Condens. Matter* **1995**, *97*, 35−47.

DOI: 10.1021/acs.chemmater.6b04505
Chem. Mater. 2016, 28, 8484−8488